High-speed silicon electro-optic modulator based on a single multimode waveguide

Gangqiang Zhou[1], Linjie Zhou[1*], Yuyao Guo[1], Shuhuang Chen[1], Zhiming Fu[2], Liangjun Lu[1], Jianping Chen[1]
[1]Shanghai Institute for Advanced Communication and Data Science, Shanghai Key Lab of Navigation and Location Services, State Key Laboratory of Advanced Optical Communication Systems and Networks, Department of Electronic Engineering, SJTU Shanghai 200240, China
[2]ZTE Photonics Technology Corporation, Fengzhan Road, Yuhuatai District, Nanjing, P.R.China, 210000
**ljzhou@sjtu.edu.cn*

Abstract: We report a novel silicon modulator that exploits the different modulation efficiency between two TE modes in a multimode waveguide. On-off key modulation was successfully demonstrated with an extinction ratio of 5.5 dB at 32 Gb/s.
OCIS codes: (130.3120) Integrated optics devices; (130.4110) Modulators.

1. Introduction

A high-speed electro-optic modulator is a key device that implements electro-optical conversion in an optical transmitter. In recent years, a lot of research has been done on silicon modulators to achieve high speed and low power consumption [1]. Mach-Zehnder interferometer (MZI) modulators and resonator-based modulators are two types of silicon modulator structures that are widely used for various modulation formats. The MZI modulators have a broadband response but the device size is relatively large. On-off keying (OOK) modulation and four-level pulse-amplitude-modulation (PAM-4) have been demonstrated with data rates up to 110 Gb/s and 90 Gb/s [2]. On the other hand, the microring modulators are much more compact but they can only operate around the resonance wavelengths and hence are more sensitive to temperature variation. OOK and PAM-4 modulations at data rates of 64 Gb/s and 128 Gb/s have been reported [3].

In this work, we present a novel silicon modulator based on a single multimode waveguide that supports two transverse electric (TE) modes. The power ratio between the two modes is adjustable by a pair of optical switches, allowing for a high static extinction ratio. A horizontal PN junction is integrated into the center of the multimode waveguide, which modulates the TE_0 mode more efficiently than the TE_1 mode. OOK modulation of 32 Gb/s is successfully demonstrated. Our device is more compact than regular MZI modulators since only a single multimode waveguide is used in the modulation section.

2. Device structure and working principle

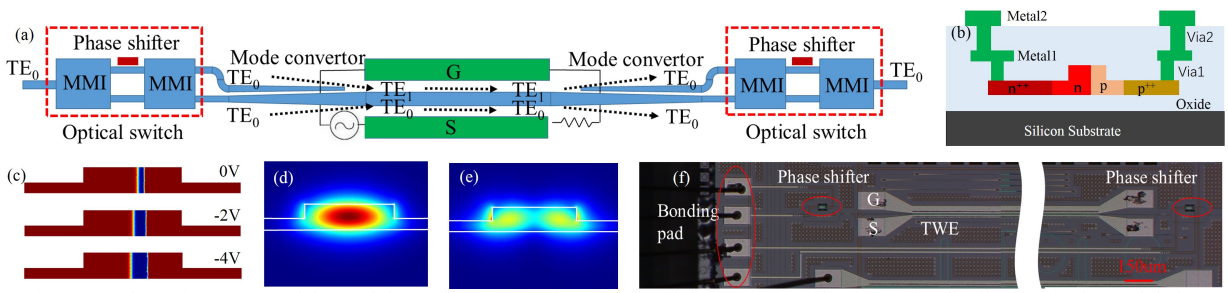

Fig. 1 (a) Schematic structure of the modulator. (b) Cross section of the modulation waveguide. (c) Carrier distributions in the modulation waveguide at three bias voltages. (d) TE_0 mode and (e) TE_1 mode profiles of the modulation waveguide. (f) Microscope image of the fabricated device.

Figure 1(a) shows the schematic structure of the modulator composed of two optical switches, two mode-converters, and a single multimode waveguide. The input light is split into two branches through the input 1×2 optical switch. The phase shifter between the multimode interferometers (MMIs) in the optical switch controls the optical power splitting ratio [4]. The TE_0 mode of one branch is converted into the TE_1 mode through a tapered mode-evolution coupler [5], and the TE_0 mode of the other branch remains unchanged. The TE_0 and TE_1 modes are phase-modulated in the multimode waveguide by the PN junction. After propagating through the multimode waveguide with different phases, the TE_1 mode is converted back into TE_0 mode through another mode converter, hence spatially separated with the TE_0 mode. The two light branches finally interfere after they pass through the output 2×1 optical switch. The phase shifter is appropriately set to get the maximum interference. The length of the multimode modulation waveguide is 3 mm.

Figure 1(b) shows the cross-section of the modulation waveguide. The waveguide width is 835 nm and the height is 220 nm with a 90 nm slab. The horizontal PN junction is formed in the center of the waveguide with a 90 nm offset to the n-doping region. The doping concentration is 4×10^{17} cm^{-3} for the p-type region and 1×10^{18} cm^{-3} for the n-type region. The heavily doped n-type and p-type concentrations are 1×10^{20} cm^{-3}. Figure 1(c) shows the free-carrier distributions in the modulation waveguide at bias voltages of 0V, -2V, and -4V. It can be seen that the PN junction depletion region is only located in the waveguide center. Figures 1(d) and 1(e) depicts the electric-field intensity profiles of the TE_0 and TE_1 modes. The TE_0 mode has an optical intensity peak in the waveguide center while the TE_1 mode has an intensity trough in the center. Therefore, the horizontal PN junction can modulate the TE_0 mode more effectively than the TE_1 mode. The phase difference between them can be changed by varying the voltage applied onto the PN junction. The interference between the TE_0 and TE_1 paths results in intensity modulation. It should be noted that the power of the two paths can be adjusted by the phase shifters so that balanced interference can be obtained. Figure 1(f) shows the microscope image of the fabricated device.

3. Simulation and experimental results

We first used the transfer matrix method to theoretically analyze the device performance. In the simulation, we assumed TE_1 path has a 6 dB higher loss than the TE_0 path to be consistent with the real device. The higher loss for TE_1 path mainly comes from the absorption from the highly-doped p^{++} and n^{++} regions, as its mode field extends laterally wider as seen from Fig. 1(e). The loss can be reduced by increasing the separation distance of the highly-doped regions. Because there is a small optical path difference caused by the phase shifter in the optical switch, the optical power splitting ratio is wavelength dependent. Figures 2 show the simulated transmission spectra of the modulator when the phase shifters in the input and output switches are properly set to get balanced interference around the 1550 nm wavelength. It suggests that a high extinction ratio is always obtainable by varying the splitting ratio.

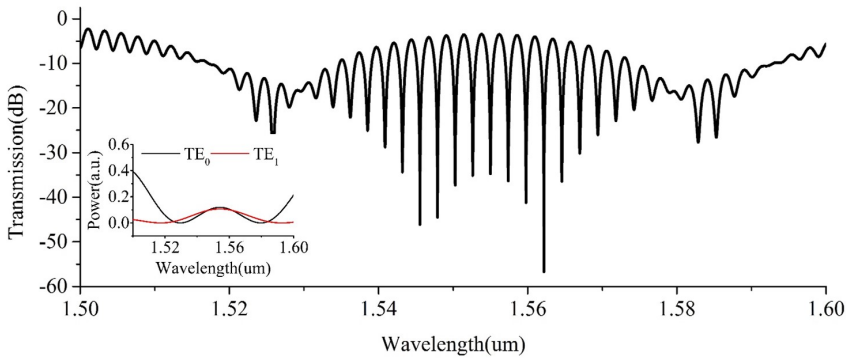

Fig. 2 Simulated transmission spectrum of the modulator. The inset shows the relative optical power of the TE_0 and TE_1 optical branches. The phases of the input and output switches are set as 0.9π and 1.7π, respectively.

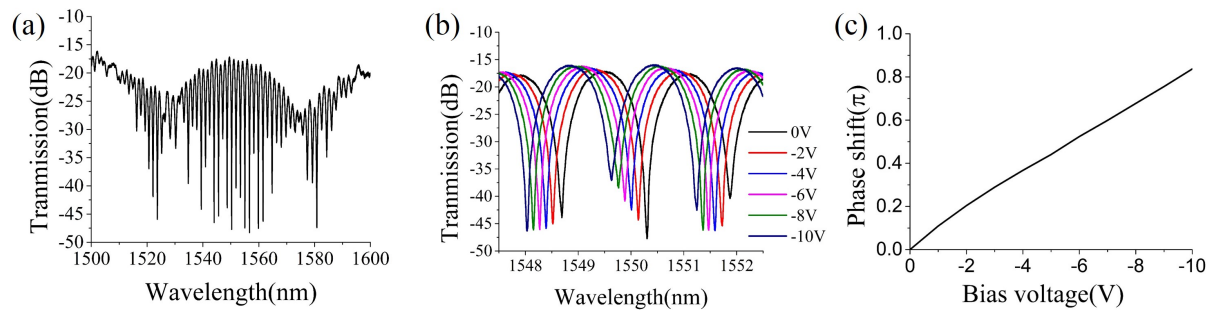

Fig. 3 (a) Measured transmission spectra of the modulator when 1.2 V/5.0 V voltages are applied to the input/output phase shifters. (b) Spectrum change with bias voltage. (c) Extracted phase shift versus bias voltage.

We next characterized the individual components in the modulator. The insertion loss (IL) of the 1×2 and 2×2 MMIs is around 0.1 dB and 0.5 dB, respectively, which could be further optimized with a lower IL of less than 0.1 dB [6]. The TE_0 mode transmission loss through the mode converter is 0.1 dB and the TE_0-TE_1 conversion loss is 0.2 dB. Figure 3(a) shows the spectrum when the voltage on the input (output) phase shifters was 1.2 V (5.0 V). The

measurement result is in good agreement with the simulation one. Figure 3(b) shows the spectrum shift under various reverse bias voltages on the PN junction. The static extinction ratio is about 30 dB at zero bias, indicating that the TE_0 and TE_1 paths take almost the equal power. Figure 3(c) shows the extracted phase shift as a function of the bias voltage. Because the width of the active arm is 835 nm and the PN junction still has a weak effect on the TE_1 mode, the modulation efficiency is lower than a regular 500-nm-wide silicon waveguide. The extracted $V_\pi \cdot L_\pi$ is 2.7 V·cm with the bias at -1V.

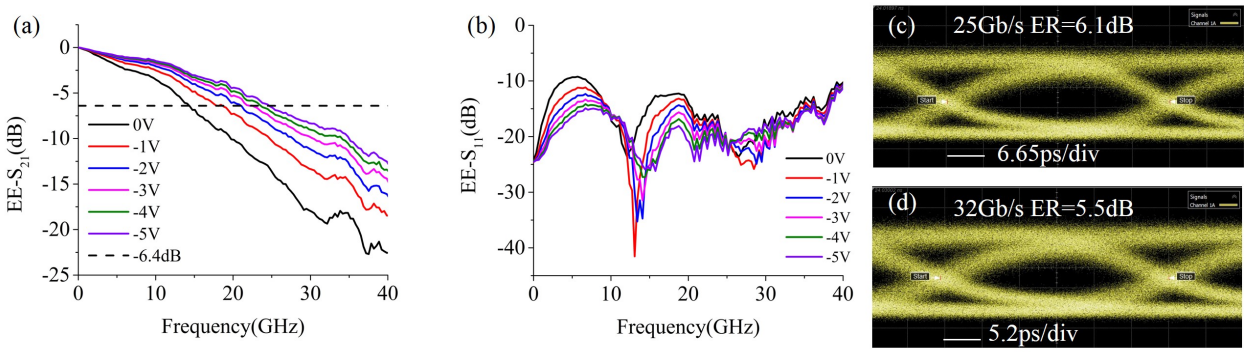

Fig. 4 (a) EE-S_{21} and (b) EE-S_{11} responses of the modulator under six bias voltages. (c, d) Eye diagrams for OOK modulation at data rates of (c) 25 Gb/s and (d) 32 Gb/s.

Figures 4(a) and 4(b) show the electro-electro (EE) S-parameter curves of the modulator measured by an Agilent 67G vector network analyzer (VNA). The measurement system was calibrated using a standard calibration procedure. The EE-S_{21} curve was normalized to the reference frequency of 10 MHz. The small-signal 6.4 dB EE bandwidth is about 14 GHz when the DC bias is 0 V and it improves to 24 GHz at a DC bias of -5 V. The EE-S_{11} curve is below -10 dB. Finally, we measured the eye-diagrams of the OOK modulation. The peak-to-peak voltage (V_{pp}) of pseudo-random binary sequence-31 (PRBS-31) signal generated from a pulse pattern generator (PPG) was amplified to 7 V by an electrical amplifier. The PRBS signal combined with the -3.5V DC voltage through a bias tee was applied to the modulator. An external 50 Ω resistor was connected to the other end of the modulator as a terminator. The modulated light was amplified by an erbium-doped optical amplifier (EDFA) and filtered by an optical filter before entering a 50 GHz photodiode (PD). Figure 4(c) and 4(d) shows the modulation results. The ER is 6.1 dB and 5.5 dB for the 25 Gb/s and 32 Gb/s OOK modulations, respectively.

4. Conclusion

We have demonstrated a silicon modulator based on one multimode waveguide integrated with a horizontal PN junction. Due to the difference in overlap between the junction depletion region and the waveguide mode profile, the TE_0 mode has a much stronger response to the modulation signal than the TE_1 mode. The static ER can be above 30 dB easily adjusted with two tunable optical switches. The preliminary results point to new ways of creating compact silicon modulators utilizing multimode silicon waveguides.

5. References

[1] G. T. Reed, G. Z. Mashanovich, F. Y. Gardes, and D. J. Thomson, "Silicon optical modulators," Nature Photonics. 4, 518–526 (2010).

[2] S. Shao, J. Ding, L. Zheng, L. Zhang, X. Fu, and L. Yang, "90 Gb/s PAM4 and OOK optical signal generation by using the dual-arm-drive silicon Mach-Zehnder modulator," in Conference on Lasers and Electro-Optics, OSA Technical Digest (online) (Optical Society of America, 2018), paper JW2A.2.

[3] J. Sun, M. Sakib, J. Driscoll, R. Kumar, H. Jayatilleka, Y. Chetrit, and H. Rong, "A 128 Gb/s PAM4 Silicon Microring Modulator," in Optical Fiber Communication Conference Postdeadline Papers, OSA Technical Digest (online) (Optical Society of America, 2018), paper Th4A.7.

[4] Q. Wu, L. Zhou, X. Sun, H. Zhu, L. Lu, J. Chen, "Silicon thermo-optic variable optical attenuators based on Mach–Zehnder interference structures," Optics Communications. 341, 69-73 (2015).

[5] J. Wang, Y. Xuan, M. Qi, L. Liu, and G. N. Liu, "Ultra-broadband integrated four-channel mode-division-multiplexing based on tapered mode-evolution couplers," 42nd European Conference on Optical Communication, Dusseldorf, Germany, 2016, pp. 1-3.

[6] P. Dumais, Y. Wei, M. Li, F. Zhao, X. Tu, J. Jiang, D. Celo, D. J. Goodwill, H. Fu, D. Geng, and E. Bernier, "2×2 multimode interference coupler with low loss using 248 nm photolithography," in Optical Fiber Communication Conference, OSA Technical Digest (online) (Optical Society of America, 2016), paper W2A.19.